Eur. Phys. J. Plus (2017) **132**: 284
DOI 10.1140/epjp/i2017-11554-1

THE EUROPEAN PHYSICAL JOURNAL PLUS

Regular Article

Growth and instability of a phospholipid vesicle in a bath of fatty acids*

J. Dervaux[1,2,a], V. Noireaux[3], and A.J. Libchaber[2]

[1] Laboratoire Matière et Systèmes Complexes, CNRS UMR 7057 Universitée Denis Diderot, 10 Rue A. Domon et L. Duquet, Paris, France
[2] Center for Studies in Physics and Biology, Rockefeller University, 1230 York Avenue, New York, NY 10021, USA
[3] School of Physics and Astronomy, University of Minnesota, Minneapolis, MN 55401, USA

Received: 13 March 2017 / Revised: 8 May 2017
Published online: 29 June 2017 –

Abstract. Using a microfluidic trap, we study the behavior of individual phospholipid vesicles in contact with fatty acids. We show that spontaneous fatty acids insertion inside the bilayer is controlled by the vesicle size, osmotic pressure difference across the membrane and fatty acids concentration in the external bath. Depending on these parameters, vesicles can grow spherically or become unstable and fragment into several daughter vesicles. We establish the phase diagram for vesicle growth and we derive a simple thermodynamic model that reproduces the time evolution of the vesicle volume. Finally, we show that stable growth can be achieved on an artificial cell expressing a simple set of bacterial cytoskeletal proteins, paving the way toward artificial cell reproduction.

1 Introduction

The RNA world hypothesis posits that the current protein-based enzymatic system at work in modern lifeforms may have originated from an RNA-based system where catalytic activities were performed by ribonucleic acids [1,2]. This hypothesis raises fundamental questions, such as how these primitive building blocks of life have reached the high concentrations that are necessary for the emergence of life. In this respect, it is thought that RNA compartmentalization within self-assembled vesicles could have allowed the formation of RNA-rich phases while avoiding the dilution of information that arises in open systems [3,4]. Because the complex machinery controlling modern cell division was not at work in protocells [3], it is reasonable to assume that environmentally controlled physico-chemical processes may have come into play to trigger protocell growth and division. Experimental studies have indeed shown that fatty acids (FA) vesicles can self-assemble [5,6], grow [7] and divide [8,9] under plausible prebiotic conditions.

Besides the relevance of these results for the origin of life, using the spontaneous ability of vesicles to divide could also provide a valuable route towards the production of self-replicating artificial cells. However, this objective requires a precise control over the growth mechanism and so far most quantitative experiments on vesicle reproduction have been performed in batch mode at the cell population level using indirect methods to detect average vesicle size and number [7,8, 10–12]. While some studies have also investigated FA/vesicles interactions using light microscopy, they have focused on the large spectra of instabilities [9,13,14] and the accurate control of spontaneous vesicle growth remains to be achieved.

With these considerations in mind, we study in this paper the interactions of individual phospholipid vesicles with a FA bath. We show that when the vesicle contains a high concentration of osmolytes, the osmotic pressure difference across the lipidic bilayer can drive the insertion of fatty acid molecules within the vesicle membrane. By monitoring in real time the growth of a single vesicle in a well-controlled environment, we have investigated the dependence of this growth process on the vesicle size, osmotic pressure difference and FA concentration in the external bath. We then derive a simple thermodynamic model that reproduces the experimental data. Next, we show that when the osmotic pressure difference across the bilayer is small, the vesicle becomes unstable at large enough external FA concentrations and spontaneously breaks into several smaller daughter vesicles. We establish the phase diagram for stable and unstable growth. Finally, we show that stable growth can be achieved on an artificial cell expressing a set of bacterial cytoskeletal proteins.

* Supplementary material in the form of 3 .avi files available from the Journal web page at http://dx.doi.org/10.1140/epjp/i2017-11554-1

[a] e-mail: dervauxjulien@wanadoo.fr

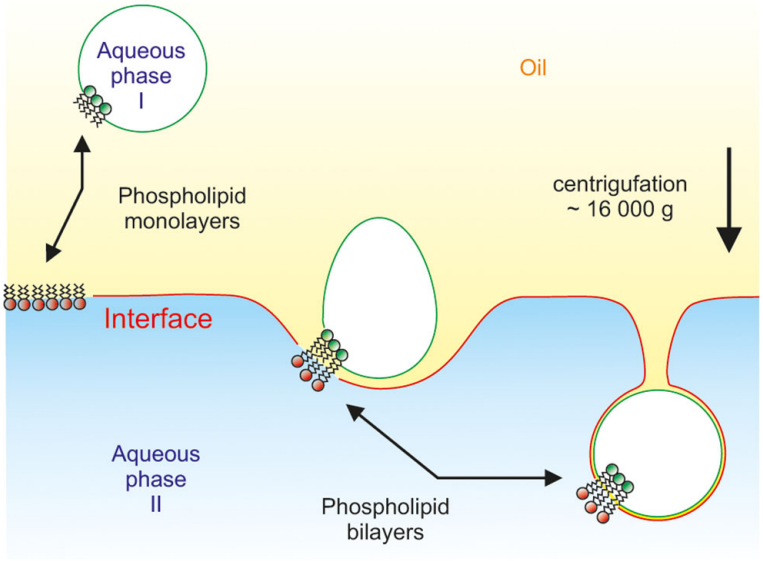

Fig. 1. Schematic representation of the vesicle production process described in the text.

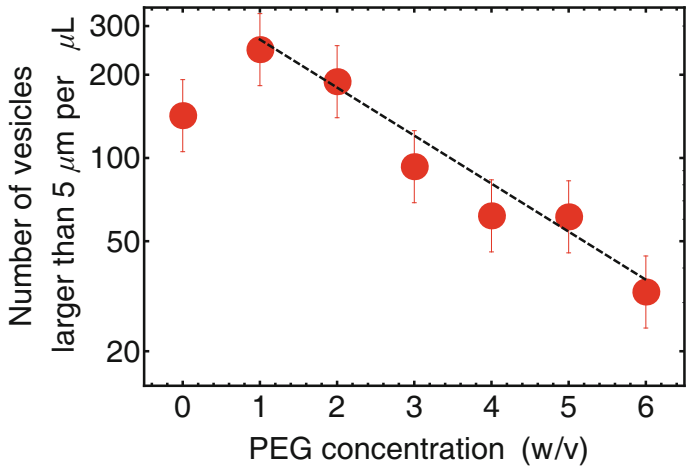

Fig. 2. Number of vesicles with diameter larger than 5 μm produced per μL as a function of the internal PEG concentration.

2 Materials and methods

2.1 Vesicle preparation

Giant unilamellar vesicles were prepared by the inverted emulsion technique [15, 16]. Briefly, Egg-PC (95%) L-α-phosphatidylcholine (Egg, Chicken - Avanti Polar Lipids) was first dispersed in mineral oil (M8410, Sigma-Aldrich) to a final lipid/oil concentration of 2mg/mL. A 2 μL droplet of phase I (6.6 mM Tris, *p*H 8.5, PEG-4500 with concentration ϕ from 0 to 6% w/v and 50 μM of the fluorescent dye AlexaFluor 488) was then added to 500 μL of the PC-oil mixture and briefly vortexed to create a dispersion of aqueous droplets stabilized by a monolayer of phospholipids. Using a wide bore pipet tip 50 μL of this emulsion was then gently laid in an Eppendorf tube on top of 20 μL of the aqueous phase II (6.6 mM Tris, *p*H 8.5). After letting the interface between the aqueous and the oil phases to stabilize for 60 s, the tube was centrifuged at 16000 g for 30 s. The centrifugation pushes the dense aqueous droplets towards the aqueous phase II and a second layer of phospholipids is added around the droplets when they cross the interface. The production process of vesicles is illustrated in fig. 1.

2.2 Vesicle yield

The efficiency of the inverted emulsion process is highly dependent on the difference of osmotic pressure between the inner and outer phases. Using a solution of polyethylene glycol (PEG) as the encapsulated aqueous solution, it can be seen on fig. 2 that the number of large ($> 5\,\mu$m) vesicles drops by an order of magnitude when the PEG concentration goes from $\sim 1.5\%$ to $\sim 6\%$.

2.3 Micelle preparation

Oleic acids micelles were prepared by first adding 10 μL of lipids (U-46-A, Nu-Check) to 1 mL of a 15 μM NaOH solution in an Eppendorf tube at 37 °C following by 1 minute vortexing and 1 hour sonication in a hot bath at 50 °C. Mixed composition micelles were prepared by first mixing oleic acid with monoolein (M239, Nu-Check) to the desired proportion. Then 10 μL of this mixture was added to 1mL of a 15 μM NaOH solution in an Eppendorf tube at 37 °C and further prepared as pure oleic acids micelles. All micelles were used within 24 hours. Final concentrations of fatty acid used in experiments are well above the cmc ($\sim 6\,\mu$M [17,18]) to avoid the dissolution of micelles.

2.4 Cell-free expression-reaction system

A previously described cell-free expression-reaction (CFER) system was used in this work [19] with minor modifications. The CFER consists of 33.3% of crude extract (9–10 mg/mL of proteins, final concentration) and 66.6% of reaction buffer and plasmids, with the following final concentrations: 50 mM HEPES *p*H 8.5, 1.5 mM ATP, 1.5 mM GTP, 0.9 mM CTP, 0.9 mM UTP, 0.2 mg/mL tRNA, 0.75 mM cAMP, 0.33 mM NAD, 0.26 mM coenzyme A, 1 mM spermidine, 0.068 mM folic acid, 1 mM DTT, 30 mM 3-phosphoglyceric acid, 1.5 mM amino acids, 3 mM Mg-glutamate, 60 mM K-glutamate, and 2% (w/v) PEG8000. A concentration of 100 μM of PEG-Rhodamine was used in the reaction to visualize the phospholipid vesicle. All of the components were purchased from Sigma-Aldrich, except GTP, CTP, UTP (USB Corporation), tRNA (Roche), and amino acids (5Primes). *E. coli* RNA polymerase and the primary sigma factor 70 were present in the extract. As previously described [20], the genes used in this study were cloned under a promoter specific to the sigma factor 28. The genes were expressed through a transcriptional activation cascade: $P_{70} \rightarrow \sigma_{28} \rightarrow P_{tar}$-gene. The promoter P_{tar} is specific to sigma 28. The plasmids used for cell-free expression were built upon the plasmid pBESTluc (Promega). The genes *mreB* and *mreC* were cloned under a P_{tar} promoter [19,21]: pBEST-P_{tar}-UTR1-*mreB* (MreB), pBEST-P_{tar}-UTR1-*yfp-mreB* (YFP-MreB), pBEST-P_{tar} UTR1-*mreC* (MreC). All of the plasmids have the highly efficient untranslated region containing the T7 *g*10 leader sequence, named UTR1 in this work [22]. The final concentrations of plasmids were as follows: 0.5 nM $P_{70} \rightarrow \sigma_{28} \rightarrow$ plasmid, 2.5 nM pBEST-P_{tar}-UTR1-*mreB* plasmid, 5 nM pBEST-P_{tar}-UTR1-*yfp-mreB* plasmid and 2.5 nM pBEST-P_{tar} UTR1-*mreC* plasmid.

2.5 Fabrication of the microfluidic device

The microfluidic photomask was designed using the CorelDraw software and printed on chrome-coated quartz masks at a resolution of 5 μm (Photo Sciences, Inc, USA). The microfluidic mold was then fabricated with polydimethylsiloxane (PDMS) using standard soft lithography techniques. Briefly, a silicon wafer (University Wafer) was cleaned with ethanol and water. After drying, the wafer was placed on a spin-coater, covered with SU-8-3025 photoresist and spun at 2000 RPM for 30 s to reach a thickness of 50 μm. The wafer was then baked for 15 minutes at 95 °C. The photoresist was then exposed to UV light for 20 minutes through the photomask. Following light exposure, the wafer was baked again for 5 minutes at 95 °C and then developed with SU-8 developer (MicroChem). Finally, the wafer was rinsed with ethanol, nanopure water and then dried. For preparation of the PDMS chips, a PDMS mixture at 10 : 1 (base : curing agent) was mixed for 3 minutes and degassed for 15 minutes in a vacuum chamber. The PDMS mixture was then poured onto the mold, degassed for 60 minutes and cured for 1 h at 80 °C. Next, the thick PDMS block was peeled off from the mold and holes were punched for the microfluidic inlets and outlets. The PDMS chip and a glass coverslip were then exposed to oxygen plasma for 30 s before bonding together and baked for at least 12 hours.

2.6 Data acquisition and analysis

Once the microfluidic chip was prepared, a solution of vesicles in aqueous phase II was injected with a syringe pump (New Era Pump Systems, Inc.) into the chip place under the microscope. Once some vesicles were trapped, the external medium was first flushed with the aqueous phase II to remove traces of unencapsulated materials. Next, FA dispersed in phase II were injected at a constant flow rate inside the microfluidic device using a syringe pump. The flow rate was adjusted to minimize vesicle deformations. Vesicle shape was monitored over time using an inverted epifluorescence microscope (Olympus IX70) equipped with appropriate fluorescence filters and a CCD camera (QImaging Retiga 1300). Images were analyzed with the software ImageJ.

3 Results

3.1 Phase diagram for a vesicle in a bath of fatty acids

Giant unilamellar vesicles (GUV) of phosphatidylcholine, encapsulating an internal aqueous phase I and immersed in an external aqueous phase II, were prepared by the inverted emulsion technique (see sect. 2). To induce vesicle growth, the GUV solution was diluted in freshly prepared oleic acid micelles dispersed in phase II (final FA concentration c

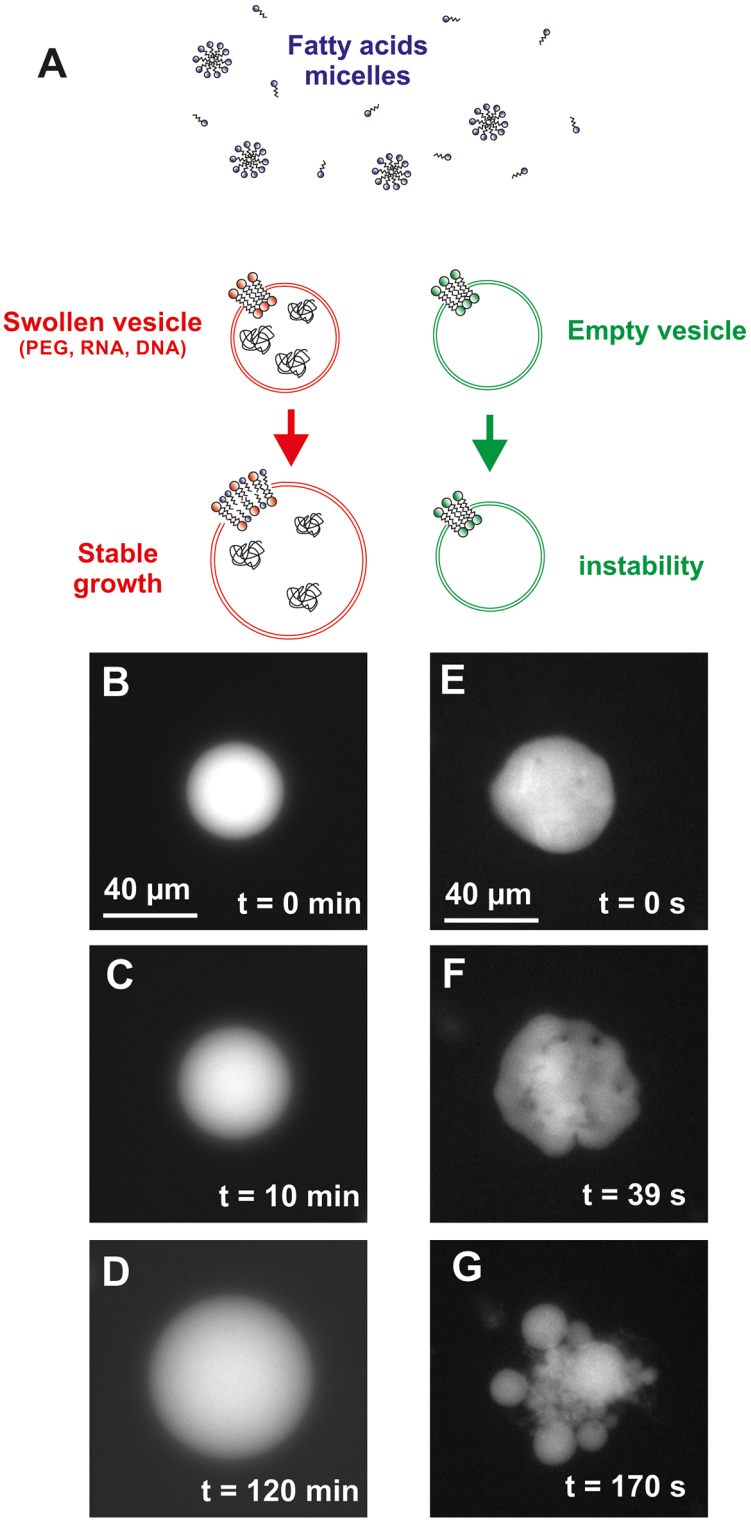

Fig. 3. (A) Schematic representation of the experiment. (B)–(D): Stable growth of a vesicle encapsulating 6% PEG immersed in a bath of FA at 160 μM. (E)–(G): Unstable growth and formation of daughter vesicles. The inner PEG concentration is 0% and the outer FA concentration is 320 μM.

between 40 μMol to 1280 μMol). The *p*H after micelle addition was 8.5. A $\sim$ 0.5 μL droplet of the GUV-FA mixture was immediately placed between two coverslips separated by a 250 μm thick spacer. The shape of large vesicles (diameter $\geq$ 10 μm) was monitored over time using an inverted fluorescence microscope and representative pictures of the experiments are presented in figs. 3(B)–(G).

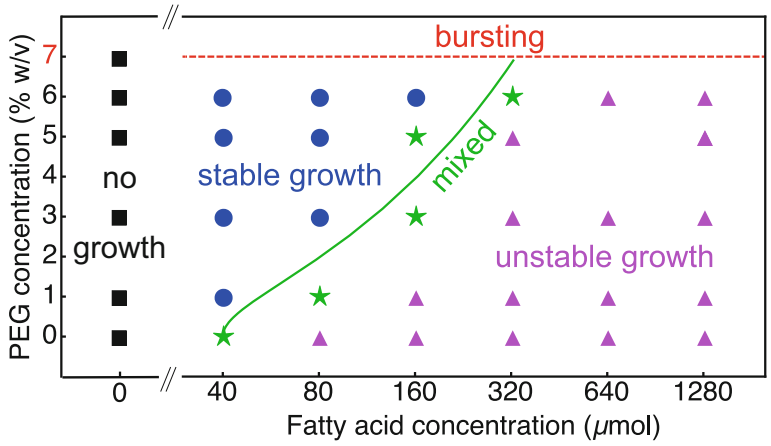

Fig. 4. Phase diagram describing the different regimes of interaction between a PEG-encapsulating GUV and a bath of FA at various concentration. The solid green line is the curve $(c \log \frac{c}{c_0})/\phi^2 = 14\,\mu$M with $c_0 = 40\,\mu$M (see model). All vesicles with internal PEG concentration of 7% bursted following FA addition.

Depending on the PEG and FA concentrations, we observed several regimes: i) at zero FA concentration, no volume or vesicle shape change was observed for all internal PEG concentrations; ii) slow stable growth retaining the spherical symmetry (figs. 3(B)–(D) and movie S1 of the Supplementary Material); iii) fast unstable growth with symmetry breaking (figs. 3(E)–(G) and movie S2 of the Supplementary Material); iv) coexistence of vesicles undergoing stable or unstable growth; and, finally, v) vesicles bursting following FA addition. Bursting events were sudden rupture of the vesicle membrane followed by dilution of the interior phase in the external phase and subsequent disappearance of the vesicle. The phase diagram in fig. 4 shows the repartition of the different regimes in the [PEG]-[FA] phase space. At high FA concentrations, in the unstable growth regime, non-spherical fluctuations of the vesicle shape are visible almost immediately (within ~ 30 seconds) following the addition of FA. The amplitude of these fluctuations increases for a few minutes until being comparable to the vesicle diameter at which point the GUV fragments into several stable small daughter vesicles.

For the largest FA concentration ($1280\,\mu$M) and internal PEG $\leq 1\%$, we also observed the formation of long tubular structures which further underwent a pearling instability, as previously reported [14]. The formation of tubular structures may be due to the generation of a spontaneous curvature in the membrane due to the relatively slow flip-flop rate of the FA molecules. In regime iv) we also observed transient instabilities where the vesicles apparently fragmented into several smaller vesicles before reincorporating them (movie S3 of the Supplementary Material). As mentioned in sect. 2, the inverted emulsion technique did not allow us to produce vesicles larger than $5\,\mu$m and containing $> 7\%$ internal PEG, presumably due to the large osmotic pressure difference across the bilayer membrane. For vesicles containing 7% internal PEG, when FA were added to the external solution (in regime v), vesicle bursting occurred. This bursting can be ascribed to the decrease in the membrane tensile strength as a result of the incorporation of FA.

3.2 Stable growth regime

We then focused on the stable growth regime and, in order to accurately characterize the growth of the vesicles for various physical parameters in a stationary environment, we used a microfluidic trap [23] to immobilize the vesicles under the microscope, as illustrated in fig. 5(A)–(C). Once some vesicles were trapped, the external medium was first flushed with the aqueous phase II to remove traces of unencapsulated materials. Next, FA dispersed in phase II were injected at a constant flow rate inside the microfluidic device using a syringe pump. The flow rate was adjusted to minimize vesicle deformations.

We first investigated the effect of vesicle size on growth. The internal PEG concentration was fixed at 6% and the fatty acids concentration at $160\,\mu$Mol. We monitored for 300 minutes the time evolution of the radius of the vesicles (with initial radii ranging from 10 to $35\,\mu$m) and plotted the results in fig. 5(D). The radii were found to increase monotonically over the course of the experiments, with up to a five-fold increase of the vesicle volume. With the continuous feeding of FA, no saturation of the growth process was observed. It can also be seen from the slopes of these curves that larger vesicles grow at faster rates than smaller vesicles. Additionally, we monitored the total fluorescence signal (integrated over the vesicle) and only a decrease of $\leq 5\%$ was measured over the course of the experiment, thus showing that dye leakage from the vesicle was minimal. Given that PEG-4500 has a larger molecular weight than the fluorescent dye (721 g/mol), this indicates that the number of PEG molecules inside the vesicle is well conserved during the growth process. Occasionally, we observed small bursts of fluorescent dye escaping from the vesicle. Because these bursts led to a sharp decrease in vesicle volume, data points after the bursts were discarded. Next, we also investigated the dependance of the growth process on the internal PEG and external FA concentrations.

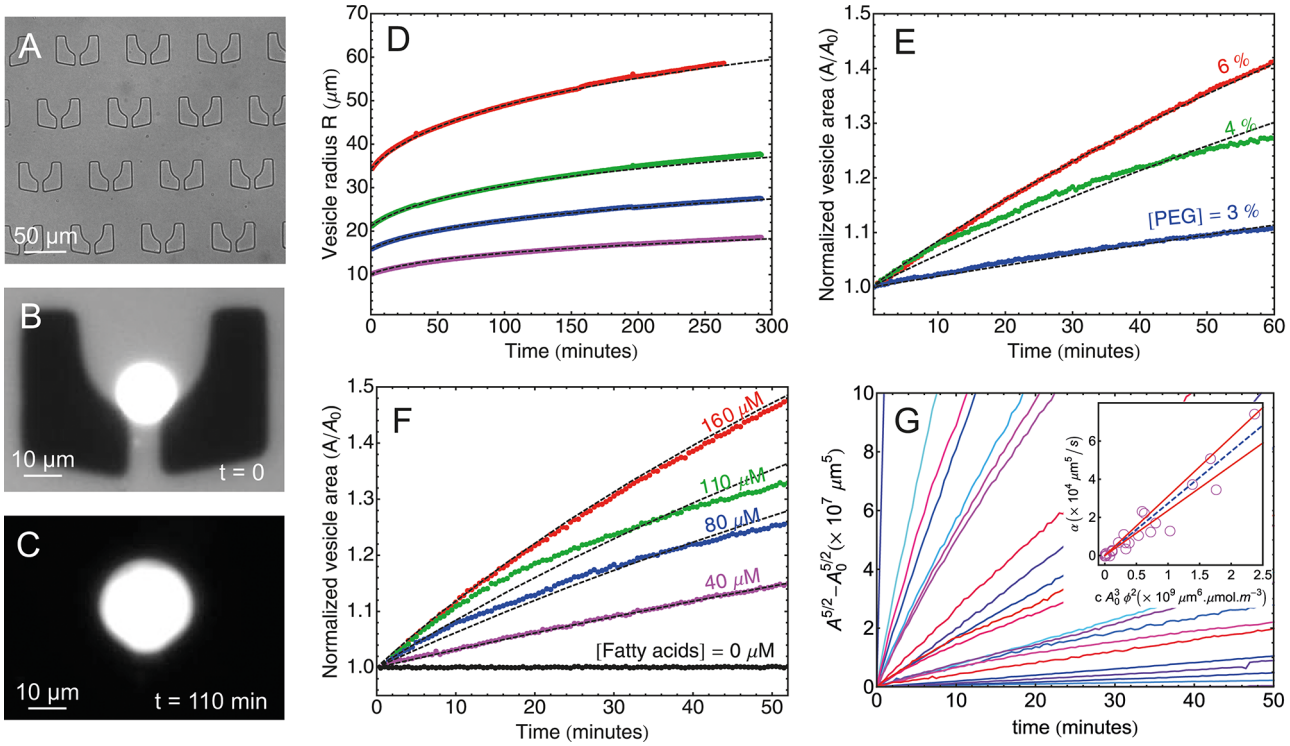

Fig. 5. (A) Microfluidic device used to trap phospholipid vesicles. Once a vesicle is trapped (B) the external medium is flushed and FA are flowed around the vesicles which grow (C). Time zero is defined as the time when FA are introduced into the microfluidic chip. (D) Time evolution of vesicle sizes for different initial radii. The internal PEG concentration is 6% and the outer FA concentration is 160 μM. (E)-(F): Time evolution of normalized vesicle areas for various internal PEG concentration (E) (FA = 80 μM) and for various outer FA concentrations (F) (inner PEG = 4%). Initial radii are $21 \pm 1\,\mu$m. (G) The rescaled areas $A^{5/2}$-$A_0^{5/2}$ show a clear linear dependence for all experiments under all conditions of stable growth investigated in this study. The slopes of these curves are proportional to $cA_0^3\phi^2$ (inset). The dashed black lines in (D), (E) and (F) are the theoretical predictions using eq. (7).

To isolate these effects from the size-dependent growth rate, vesicles with similar diameter (within 5%) were selected and their growth was monitored over $\sim$ 50 minutes. The time evolution of their area A (scaled by their respective initial area A_0) is plotted in fig. 5(E)–(F) for various values of the control parameters. Increasing the PEG or FA concentrations increased the vesicle growth rate. Growth could also be induced by replacing the internal PEG by single (90 thymine sequences at a concentration of 2.5% w/v) or double-stranded (λ-phage genomic DNA at a concentration of 2.5% w/v) DNA (data not shown).

3.3 Theoretical model

To analyze these data, we now write a simple thermodynamical model describing the osmotically driven growth of a phospholipid vesicle of radius R in contact with a reservoir of fatty acids at molar concentration c. In all generality, fatty acids (FA) and solvent particles migrate from the external bath to the membrane bilayer or to the vesicle interior if this decreases the Gibbs free energy of the system. If the migration of solvent particles is fast compared to the migration of the FA, the vesicle remains swollen and spherical. On the other hand, if FA incorporation in the membrane bilayer exceeds the permeation of the membrane by solvent particles, the area A of the vesicle may grow faster than its volume V and we can expect the vesicle to become floppy and to lose its sphericity. In order to first describe the stable growth regime, we shall make the assumption that the migration of solvent molecules is fast enough for the vesicle to remain spherical. Under this assumption, the total number N of FA molecules in the membrane is governed by the mass conservation equation: $\partial N/\partial t = A(J_{\rm ext} - J_{\rm int})$ where $J_{\rm ext}$ and $J_{\rm int}$ are, respectively, the flux of FA molecules from the external bath to the membrane and from the membrane toward the vesicle interior. However, because we expect that the FA concentration at equilibrium will be roughly the same inside and outside the vesicle, the total number of FA molecules inside the vesicle (around 10^5–10^6 for a 20 μm diameter vesicle in a 100 μM bath) will be negligible compared to the total number of FA molecules in the membrane (around 10^9 for a 10 μm diameter vesicle doubling its area and assuming that the area per molecule is $a = 30\,\text{Å}^2$) and we shall neglect the flux $J_{\rm int}$ in the following. According to Fick's law, the flux $J_{\rm ext}$ is related to the change in chemical potential by $J_{\rm ext} = \mathcal{N}cD/\ell k_B T(\mu_{\rm ext} - \mu_{\rm ves})$ associated with the insertion of a FA molecule inside the vesicle membrane. $\mathcal{N}$, D, k_B and T are, respectively, the Avogadro

constant, FA diffusion coefficient, Boltzmann constant and temperature. ℓ is a lengthscale that we will discuss later. In the external bath the chemical potential $\mu_{\rm ext}$ of the FA is simply that of an ideal solution $\mu_{\rm ext} = \mu_0 + k_B T \log \frac{c}{c_0}$. Here μ_0 is the reference chemical potential at the reference concentration c_0 and c is the FA concentration in the external bath. The chemical potential $\mu_{\rm ves}$ is related to the change in Gibbs free energy $G_{\rm ves}$ of the vesicle by $\mu_{\rm ves} = \partial G_{\rm ves}/\partial N$ associated with a variation of the number N of FA in the vesicle membrane. In the limit of fast water transport, $G_{\rm ves}$ contains two contributions: i) a membrane term describing the cost of inserting FA inside the bilayer and ii) a volume term accounting for the dilution of the polymers inside the vesicle due to the increase in area. We then write

$$\mu_{\rm ves} = \frac{\partial G_{\rm ves}}{\partial N} = \underbrace{\frac{\partial G_{\rm layer}}{\partial N}}_{\mu_{\rm layer}} + \underbrace{\frac{\partial G_{\rm vol}}{\partial N}}_{\mu_{\rm vol}} . \tag{1}$$

Using the Flory-Huggins energy to model the solvent-polymer mixture inside the vesicle, $G_{\rm vol}$ is given by

$$G_{\rm vol} = k_B T N_p \log \frac{N_p v_p}{V} + k_B T N_s \log \frac{N_s v_s}{V} . \tag{2}$$

Here N_p and N_s are, respectively, the number of polymer and solvent molecules and v_p and v_s are, respectively, the volume of polymer and solvent molecules. Molecular incompressibility implies $v_s N_s + v_p N_p = V$ and the fixed number of polymer molecules can be written as $N_p = \phi V_0/v_p$, where V_0 is the initial volume and ϕ is the initial volume fraction of polymer. Finally, using the fact that $V = A^{3/2}/6\sqrt{\pi}$ and the relation between the total area and number of FA in the membrane $A = A_0 + aN$, the chemical potential $\mu_{\rm vol} = \partial G_{\rm vol}/\partial N$ is

$$\mu_{\rm vol} = \frac{a k_B T}{4 v_s} \sqrt{\frac{A}{\pi}} \left\{ \log \left(1 - \phi \left(\frac{A_0}{A} \right)^{\frac{3}{2}} \right) + \phi \left(\frac{A_0}{A} \right)^{\frac{3}{2}} \right\} . \tag{3}$$

Given the rather low polymer concentration in our experiments, ($\phi < 6\%$), we can use the fact that $\phi (A_0/A)^{3/2} \ll 1$ and thus

$$\mu_{\rm vol} \approx - \frac{a k_B T A_0^3 \phi^2}{8\sqrt{\pi} v_s A^{5/2}} . \tag{4}$$

Finally, plugging these results in the mass conservation equation, we get the following differential equation for the area A of the vesicle:

$$\frac{\partial A}{\partial t} = A \frac{\mathcal{N} a c D}{\ell k_B T} \left(\mu_{\rm ext} - \mu_{\rm layer} \right) + \underbrace{\frac{\mathcal{N} a^2 c D A_0^3 \phi^2}{8\sqrt{\pi} \ell v_s}}_{\alpha} \frac{1}{A^{3/2}} , \tag{5}$$

where $\mu_{\rm layer} = \partial G_{\rm layer}/\partial N$. Because experimental data show that vesicle growth is very small at low internal polymer concentration, we neglect the membrane term and only consider the osmotically driven contribution to the growth process. More quantitatively, if $(\mu_{\rm ext} - \mu_{\rm layer})$ is of order $\sim k_B T$ and the area A is of order $\sim A_0$, the ratio of the first to the second term in the right-hand side of eq. (5) is $8\sqrt{\pi} v_s / a \sqrt{A_0} \phi$. For a vesicle with a diameter of $20\,\mu$m, this ratio is less than 10^{-3} and our assumption to neglect the first term in (5) is thus appropriate. Using the Flory-Huggins energy to model the solvent-polymer mixture inside the vesicle, the time evolution of the vesicle area is described by the following nonlinear differential equation (see sect. 2):

$$\frac{\partial A}{\partial t} = \underbrace{\frac{\mathcal{N} a^2 c D A_0^3 \phi^2}{8\sqrt{\pi} \ell v_s}}_{\alpha} \frac{1}{A^{3/2}} , \tag{6}$$

where ϕ is the initial volume fraction of polymer and v_s the volume of a solvent molecule. This nonlinear differential equation, supplemented by the initial condition $A(0) = A_0$, has the following solution:

$$A = \left(A_0^{\frac{5}{2}} + \frac{5}{2} \alpha t \right)^{\frac{2}{5}} . \tag{7}$$

In order to check the functional time-dependance of the vesicle area, we plotted the quantity $A^{\frac{5}{2}} - A_0^{\frac{5}{2}}$ for all data curves. As can be seen on fig. 5(G), these curves show a clear linear time dependance. The slopes of these curves were then extracted and plotted against $c A_0^3 \phi^2$ (inset of fig. 5(G)). The linear slope of this curve reveals a nice agreement of the data with the theoretical model and gives $\mathcal{N} a^2 D/(8\sqrt{\pi} \ell v_s) = 2.7 \pm 0.2 \times 10^{10}\,{\rm m}^5/{\rm s}$. Using typical

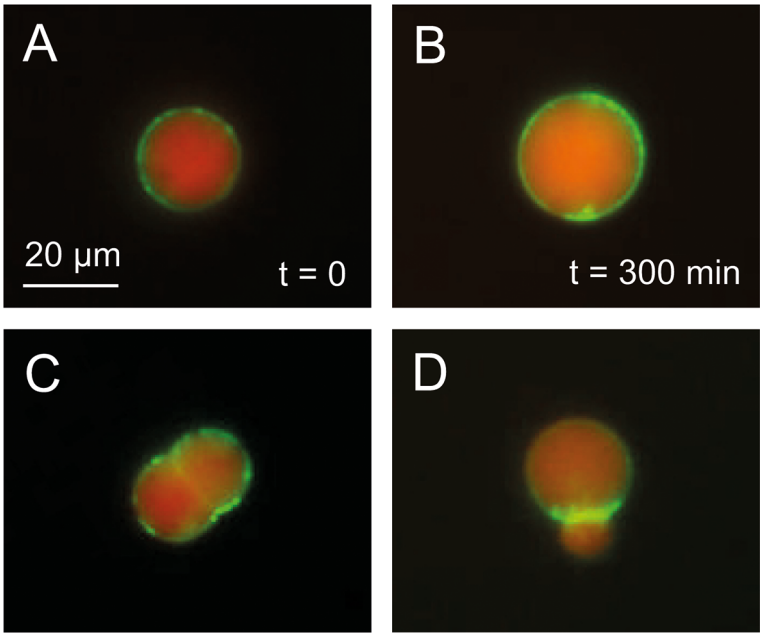

Fig. 6. Growth of vesicles encapsulating a CFER system and expressing the proteins MreB, yfp-MreB and MreC. (A) Before growth, the MreB protein (false-colored green) is localized at the membrane surface and the interior of the GUV is tagged with PEG-rhodamine (false-colored red). (B) Addition of a mixture of FA led to stable growth of the artificial cell. In the experiment shown here, the vesicle volume is ~ 2.2 times its initial volume after 300 minutes of growth. (C) and (D) Two examples of budded vesicles after 300 minutes of growth. These initially spherical vesicles have lost their sphericity because of the geometrical constraint due to the network of cytoskeletal protein beneath the membrane.

values ($a = 30\,\text{Å}^2$, $D = 10^{-10}\,\text{m}^2/\text{s}$, $v_s = 3.10^{-30}\,\text{m}^3$), this yields a value for the thickness ℓ of $\sim 2\,\mu$m. This result indicates that the relevant lengthscale for FA transport is not the bilayer thickness but rather the thickness of the diffusive boundary layer, *i.e.* the lengthscale of the concentration gradient between the bath and the membrane. Note that this result might be different for larger molecules, such as phospholipids, for which the insertion step is slower than for FA. At higher FA (or lower PEG) concentration, the first term in eq. (5) cannot be neglected anymore. As vesicle size will increase, the osmotic pressure difference that drives the insertion of water molecules inside the vesicles will decrease. In that case, the hypothesis that fatty acids insertion is the limiting factor of vesicle growth will likely break down at some point. In that case, it will become necessary to take into account the kinetics of the permeation of water molecules inside the vesicles. While a full model of coupled water and FA transports is outside the scope of this paper, we can estimate the relative influence of these two terms. At high FA concentration, the driving force for FA insertion is the difference in chemical potential between the exterior and the vesicle membrane. Because the latter does not depend on the external FA concentration c, this driving force will behave as $c \log \frac{c}{c_0}$, at high enough c. The osmotic driving force for water molecules on the other hand behaves as ϕ^2 and we can thus expect that stable growth will occur when $(c \log \frac{c}{c_0})/\phi^2$ is below a critical value while growth will become unstable when this ratio is above the critical value. Using $c_0 = 40\,\mu$M, we find that the curve $(c \log \frac{c}{c_0})/\phi^2 = 14\,\mu$M indeed partitions the phase diagram into stable and unstable regions.

3.4 Growth of vesicles expressing membrane proteins

Next, we investigated the feasibility of achieving stable growth on vesicles expressing a set of cytobacterial proteins [20]. To this end, we encapsulated an efficient cell-free expression-reaction (CFER) system containing all the necessary components for transcription and translation inside the GUV [19, 21]. Two key proteins of the *E. coli* cytoskeleton, MreB and MreC were cloned inside individual plasmids and expressed concurrently. A third plasmid containing a yfp-tagged MreB protein was also expressed to visualize the formation of this simplified cytoskeleton on the vesicle membrane. The vesicle interior was detected by incorporating $100\,\mu$M of PEG-rhodamine to the CFER. Because oleic acids precipitate at concentration of cations smaller than those required for gene expression, we used a mixture of oleic acid and monoolein (at ratio 2 : 1) to stabilize the FA micelles. Furthermore, FA insertion inside the GUV critically relies on a *p*H of ~ 8.5. Because gene expression at this *p*H is sub-optimal, $1\,\mu$M of the pore-forming protein α-hemolysin from *Staphylococcus aureus* was added to the external medium to create a permeability of the vesicles to nutrients. This compensated for the sub-optimal *p*H and enhanced protein production inside the GUV. After 12 hours of gene expression, a layer of MreB proteins could be seen on the vesicle membrane (fig. 6(A)). GUVs were then

transferred in a solution containing a mixture of FA at $60\,\mu$M and the volume of these vesicles doubled within 300 minutes as seen in fig. 6(B). While several vesicles grew successfully, other vesicles bursted upon FA addition as did all the vesicles at higher ($\geq 160\,\mu$M) FA concentrations, even when the osmotic pressure difference was lowered by adding PEG to the external medium. Consequently, the unstable growth mode, with fast and large fluctuations of the vesicle shape, could not be triggered. However, in some instances, the cortex of cytoskeletal proteins prevented the radially symmetric growth of the vesicles. In those cases (fig. 6(C) and (D)), growth led to the formation of buds and a loss of the radial symmetry, as in the unstable growth mode seen on the model system.

4 Conclusions

Using a model system of a phospholipid vesicle immersed in a well-controlled stationary bath of fatty acids, we have shown that vesicle growth or division are two processes controlled by the external fatty acids concentration and the osmotic pressure difference across the membrane, but also, quite surprisingly, strongly dependent on the size of vesicles. In our study, the osmotic pressure was controlled by tuning the PEG concentration inside the vesicles but similar results are expected if using other molecules (such as sugars) to which the vesicle membrane is impermeable. We have developed a theoretical model describing the insertion of fatty acids into osmotically swollen vesicles that closely reproduces the experimental data, including the dependence of the growth process on the vesicle size. In order to fully describe the phase diagram presented in this work and in particular the emergence of unstable non-spherical modes at large fatty acid concentrations, more theoretical work is needed to describe the coupled transport of fatty acids and solvent molecules. Further experimental work is also needed to understand the unstable growth process and, in particular, the size distribution of the daughter vesicles. Moreover, the finite size of the microfluidic trap used in our experimental setup did not allow us to observe the behavior of vesicles at very large time. Therefore the long-time stability and growth behavior of vesicles remains an open question. Since the results presented in this work have highlighted that vesicle size is an important parameter controlling vesicle growth, it would also be interesting to investigate how a population of vesicles evolve when external resources such as fatty acids are limited. Indeed, does evolution select a characteristic vesicle size in such a system?

Next we have shown that slow stable growth could be induced on vesicles encapsulating a cell-free expression-reaction system. Although fast unstable growth leading to vesicle fragmentation could not be induced in this system, the presence of cytoskeletal proteins was able to induce bud formation during growth. Therefore, in order to trigger artificial cell division by taking advantage of the unstable growth mechanism described in this study, as observed in L-shape bacteria [24], it will be necessary to find more stable combinations of fatty acids. Alternatively, an additional forcing could be provided to separate buds from mother vesicles. For example, experiments have shown that contractile forces are produced spontaneously when the FtsZ protein ring is reconstructed inside liposomes [25]. Expressing this protein together with the primitive cytoskeleton described here could provide a possible mechanism of artificial cell division.

AL and VN acknowledge support from HFSP account RGP 0037/2015.

Author contribution statement

JD, AL and VN conceived and designed the experiments, analyzed the data and wrote the paper. JD performed the experiments. JD, AL and VN contributed reagents/materials/analysis tools.

References

1. R.F. Gesteland, T.R. Cech, J.F. Atkins (Editors), *The RNA World*, 2nd edition (Cold Spring Harbor Press, Cold Spring Harbor, 1998).
2. L.E. Orgel, Crit. Rev. Biochem. Mol. Biol. **39**, 99 (2004).
3. J.W. Szostak, D.P. Bartel, P.L. Luisi, Nature **409**, 387 (2001).
4. I.A. Chen, P. Walde, Cold Spring Harb. Perspect. Biol. **2**, a002170 (2010).
5. J.M. Gebicki, M. Hicks, Nature **243**, 232 (1973).
6. W.R. Hargreaves, D.W. Deamer, Biochemistry **17**, 3759 (1978).
7. M.M. Hanczyc, S.M. Fujikawa, J.W. Szostak, Science **302**, 618 (2003).
8. P. Walde, R. Wick, M. Fresta, A. Mangone, P.L. Luisi, J. Am. Chem. Soc. **116**, 11649 (1994).
9. T.F. Zhu, J.W. Szostak, J. Am. Chem. Soc. **131**, 5705 (2009).
10. I.A. Chen, R.W. Roberts, J.W. Szostak, Science **305**, 1474 (2004).

11. I.A. Chen, J.W. Szostak, Biophys J. **87**, 988 (2004).
12. Markvoort *et al.*, Biophys. J. **99**, 1520 (2010).
13. P. Peterlin, V. Arrigler, K. Kogej, S. Svetina, P. Walde, Chem. Phys. Lipids **159**, 67 (2009).
14. C. Hentrich, J.W. Szostak, Langmuir **30**, 14916 (2014).
15. S. Pautot, B.J. Frisken, D.A. Weitz, Langmuir **19**, 2870 (2003).
16. V. Noireaux, A. Libchaber, Proc. Natl. Acad. Sci. **101**, 17669 (2004).
17. G.V. Richieri, R.T. Ogata, A.M. Kleinfeld, J. Biol. Chem. **267**, 23495 (1992).
18. B.M. Davis, J. Richens, P. O'Shea, Biophys. J. **101**, 245 (2011).
19. J. Shin, V.J. Noireaux, Biol. Eng. **4**, 8 (2010).
20. Y.T. Maeda, T. Nakadai, J. Shin, K. Uryu, V. Noireaux, A. Libchaber, ACS Synth Biol. **1**, 53 (2012).
21. J. Chalmeau, N. Monina, J. Shin, C. Vieu, V. Noireaux, Biochim. Biophys. Acta **1808**, 271 (2011).
22. P.O. Olins, C.S. Devine, S.H. Rangwala, K.S. Kavka, Gene **73**, 227 (1988).
23. A. Huebner *et al.*, Lab Chip **9**, 692 (2009).
24. R. Mercier, Y. Kawai, J. Errington, Cell **152**, 997 (2013).
25. M. Osawa, D.E. Anderson, H.P. Erickson, Science **320**, 792 (2008).